

Ligand Spheres in asymmetric hetero Diels-Alder reactions catalyzed by Cu(II) box complexes: Experiment and Modeling

V. Umamaheswari,^[a] Pawel Cias,^[a] Andreas Pöppl,^[b] Martin Kaupp,^[c]
and Georg Gescheidt ^{*[a]}

^[a] Institute for Physical and Theoretical chemistry, Graz University of Technology,

Stremayrgasse 9, 8010 Graz, Austria

^[b] Faculty of Physics and Earthscience, University of Leipzig, Linnéstr. 5, D-04103 Leipzig,

Germany

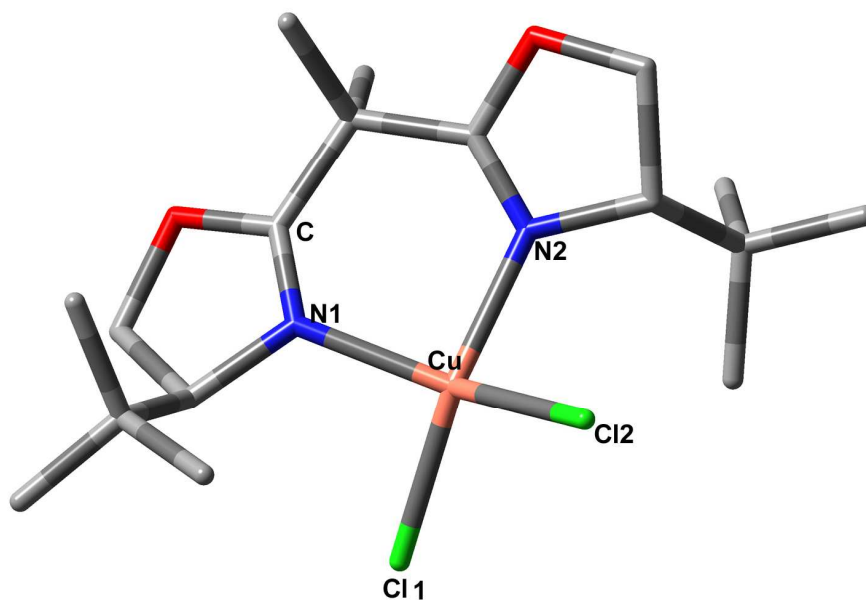
^[c] Technische Universität Berlin, Fakultät II, Institut für Chemie, Strasse des 17. Juni 135, 10623

Berlin, Germany

Supplementary Information

Contents

1. Comparison between the calculated geometry and the X-ray structure of CuboxCl₂.
2. EPR, ENDOR, and HYSCORE spectra together with the positioning of the tensor axes.
3. Experimental and computed g-factors of the model structures.
4. Experimental/simulated and computed HFC couplings for **LP1**, **LP2** and **LP3** structures.



	X-ray (Ref 35)	B3LYP/TZVP
Cu-N1	198	200
Cu-Cl1	223	224
N1-Cu-N2	90.5	90.9
Cl1-Cu-Cl2	99.8	98.9
C-N1-Cu-Cl2	108.9	109.8

Figure/Table S1: Experimental and calculated geometry of CuboxCl₂. Hydrogen atoms are omitted for clarity. Distances are given in pm, angles in °.

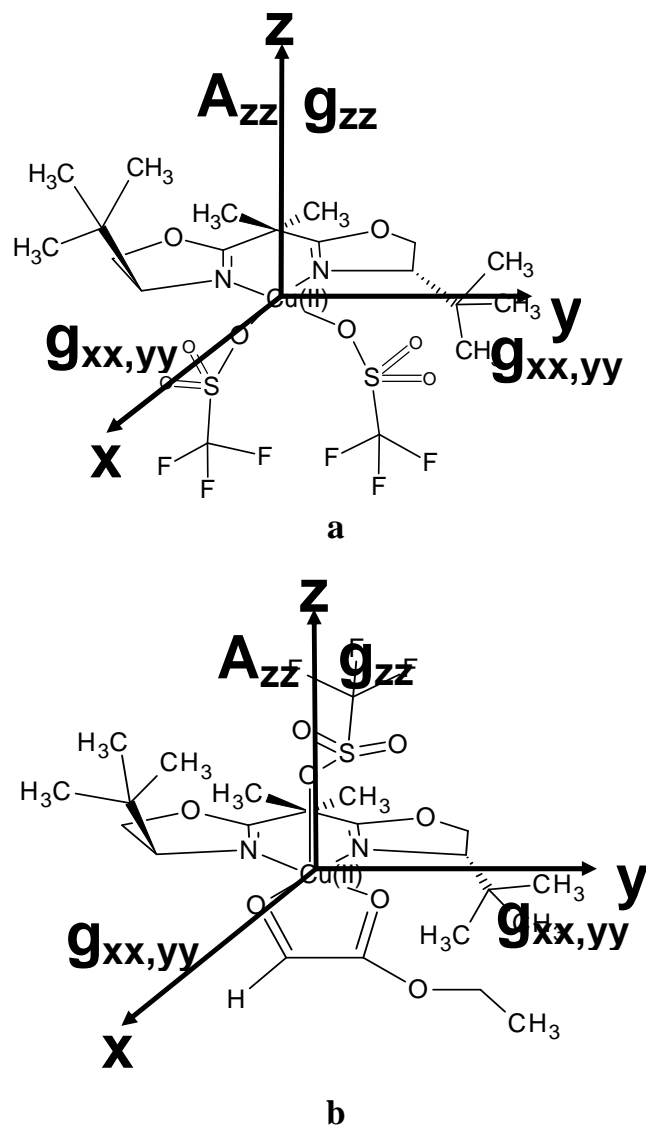


Figure S2. Tensor diagram showing the orientation of the principal axes frames with respect to the (a) distorted square planar complex structure for Stage 1 (**S1**) - $\text{Cu}(\text{OTf})_2/\text{tert-butylbox}$ and (b) distorted square pyramidal complex structure for Stage 2 (**S2**) - $\text{Cu}(\text{OTf})_2/\text{tert-butylbox}$ + ethyl glyoxylate and Stage 3 (**S3**) - $\text{Cu}(\text{OTf})_2/\text{tert-butylbox}$ + ethyl glyoxylate + 1,3-cyclohexadiene (1,3-cyclohexadiene is not included in the picture since it is not directly coordinated to the Cu(II) center)

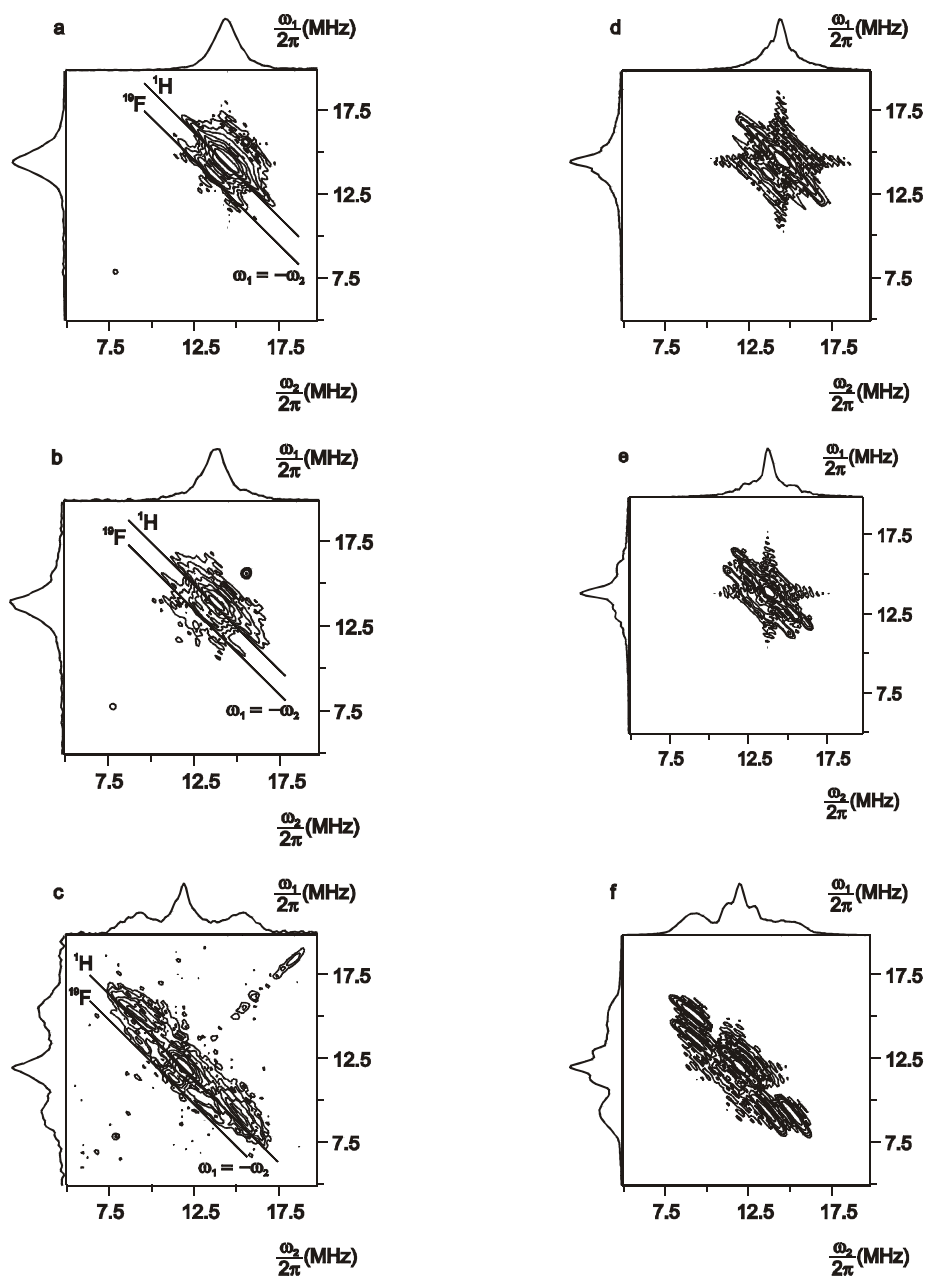


Figure S3. Added X- band HYSCORE spectra of stage 1 (S1) - $\text{Cu}(\text{OTf})_2/\text{tert-butylbox}$, measured at 4 K, (a) 339.5 mT, $\tau = 104 + 160 + 32$ ns (b) 325.5 mT, $\tau = 104 + 160 + 32$ ns (c) 281.5 mT, $\tau = 160 + 40$ ns at 4 K, (a, b, c – Experimental) and (d, e, f – Simulated)

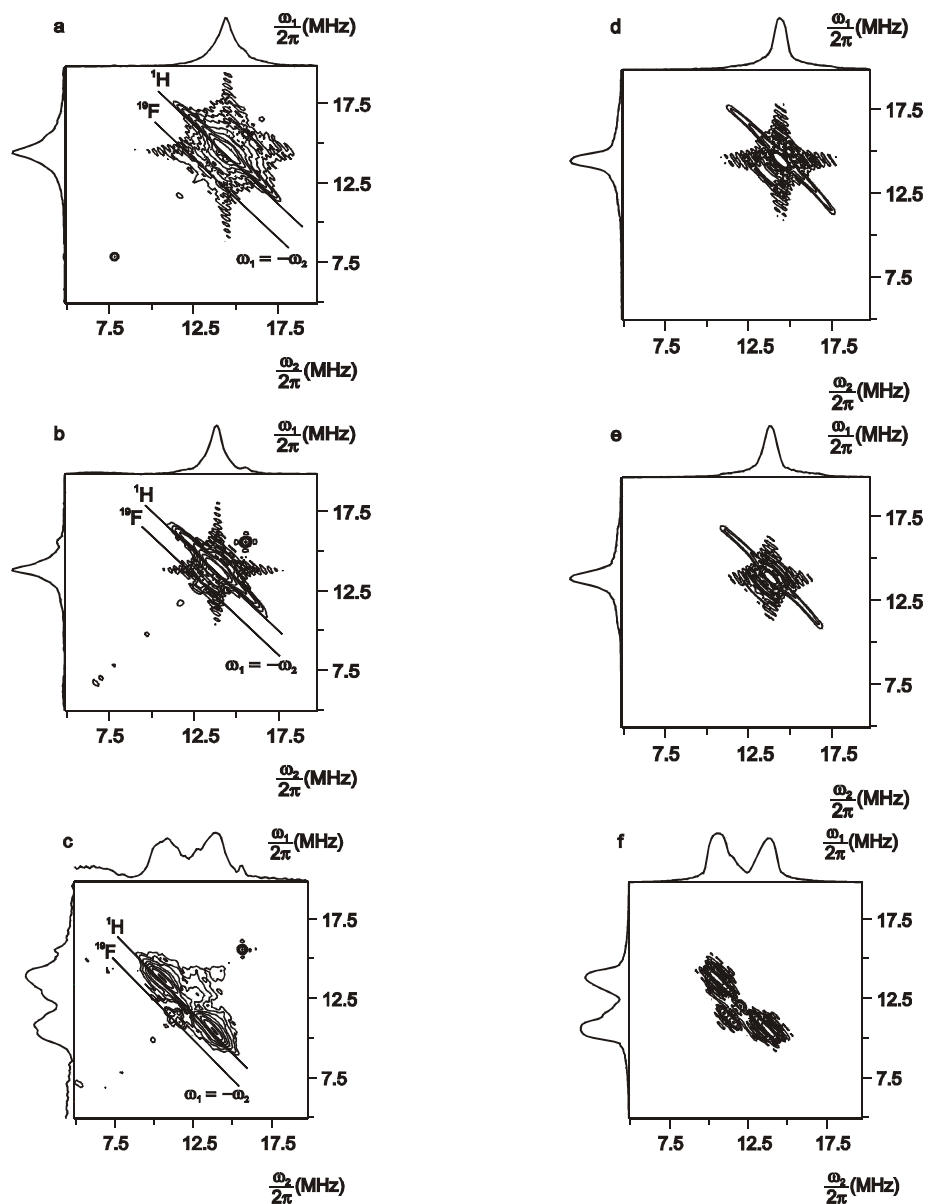


Figure S4. X- band HYSCORE spectra of stage 3 (S3) - Cu(OTf)₂/tert-butylbox + ethyl glyoxylate + 1,3-cyclohexadiene (a) 339.5 mT, $\tau = 104 + 160 + 32$ ns (b) 325.5 mT, $\tau = 104 + 160 + 32$ ns (c) 281.5 mT, $\tau = 160$ ns at 4 K, (a, b, c – Experimental) and (d, e, f – Simulated)

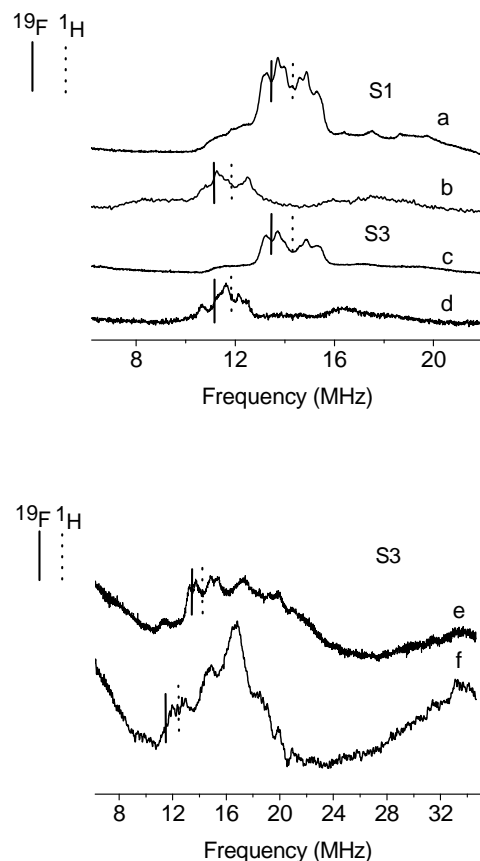


Figure S5. X- band Experimental Davies ENDOR spectra of **S1** – Cu(OTf)₂/tert-butylbox (a – 335.4 mT and b – 278.5 mT), and **S3** - Cu(OTf)₂/tert-butylbox + ethyl glyoxylate + 1,3-cyclohexadiene (c – 335.4, d – 278.5 mT), measured at 4 K with long microwave pulses of $t_{\pi/2} = 96$ and $t_{\pi} = 192$ ns, and (e – 335.4 mT) and (f – 290 mT) of **S3** measured with short microwave pulses $t_{\pi/2} = 16$ and $t_{\pi} = 32$ ns

This hf contrast selective ENDOR experiments for **S3** prove unambiguously the presence of broad ¹⁴N ENDOR signals in the range 16 MHz – 24 MHz (spectrum in Fig. S5 /e/ recorded at 335.4 mT) and 16 MHz – 20 MHz (Fig. S5 /f/ recorded at 290.0 mT). The data provide a rough estimate of $A_{\parallel}^N \approx 48$ MHz and $A_{\perp}^N \approx 32$ MHz for the ¹⁴N hfc parameters in sample III. Note that the largest ¹⁴N hfc is observed in the ENDOR spectrum taken at 335.4 mT (Fig. S5 /e/). Therefore, the A_{\parallel}^N principal axis of the ¹⁴N hfc tensor lies within the x-y plane of the Cu(II) g tensor. In the same way we may likewise assign the broad baseline signals ranging from 17 MHz to 20 MHz in the ENDOR spectra of sample I (Fig. S5 /a and b/) to ¹⁴N signals yielding hfc estimates of $A_{\parallel}^N \approx 40$ MHz and $A_{\perp}^N \approx 34$ MHz for the respective hfc parameters.

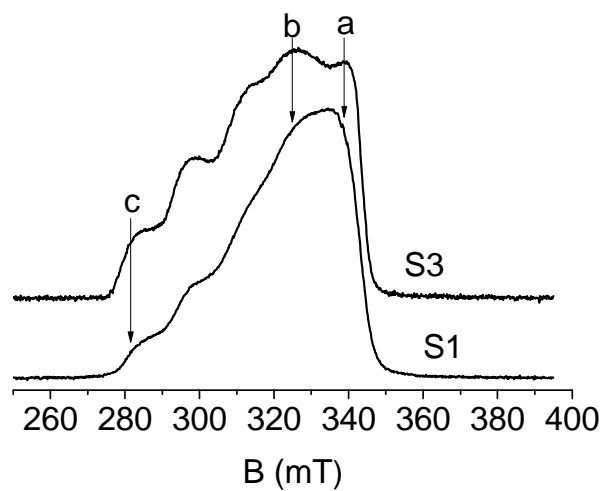


Figure S6. X- band two pulse field-swept ESE spectra measured with short pulses $\pi/2 = 16$ ns and $\pi = 32$ ns, and the pulse delay of $\tau = 800$ ns at 4 K, of **S1** - $\text{Cu}(\text{OTf})_2/\text{tert}$ -butylbox and **S3** - $\text{Cu}(\text{OTf})_2/\text{tert}$ -butylbox + ethyl glyoxylate (**1**) + 1,3 - cyclohexadiene (**2**), the arrows with a, b and c represents the fields 339.5 mT, 325.5 mT and 281.5 mT respectively, at which the HYSCORE spectra were measured.

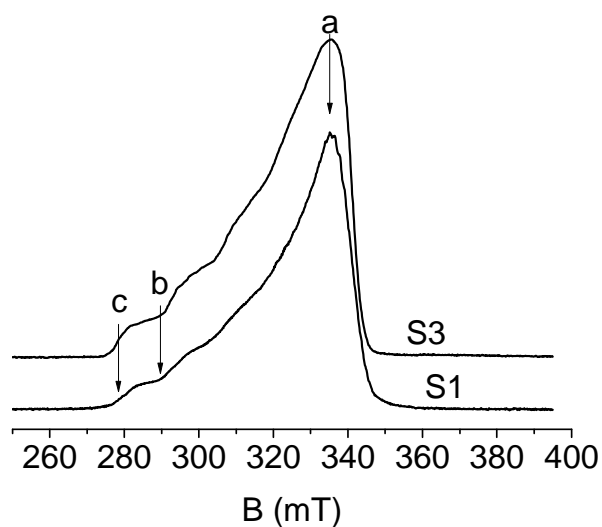


Figure S7. X- band two pulse field-swept ESE spectra measured with the selective microwave pulses of $t_{\pi/2} = 96$ ns and $t_{\pi} = 192$ ns, and with the pulse delay of $\tau = 1200$ ns, at 4 K, of S1 - Cu(OTf)₂/*tert*-butylbox and Stage 3 (S3) - Cu(OTf)₂/*tert*-butylbox + ethyl glyoxylate (**1**) + 1,3 - cyclohexadiene (**2**), the arrows with a, b and c represents the fields 335.4 mT, 290 mT and 278.5 mT respectively, at which the ENDOR spectra were measured

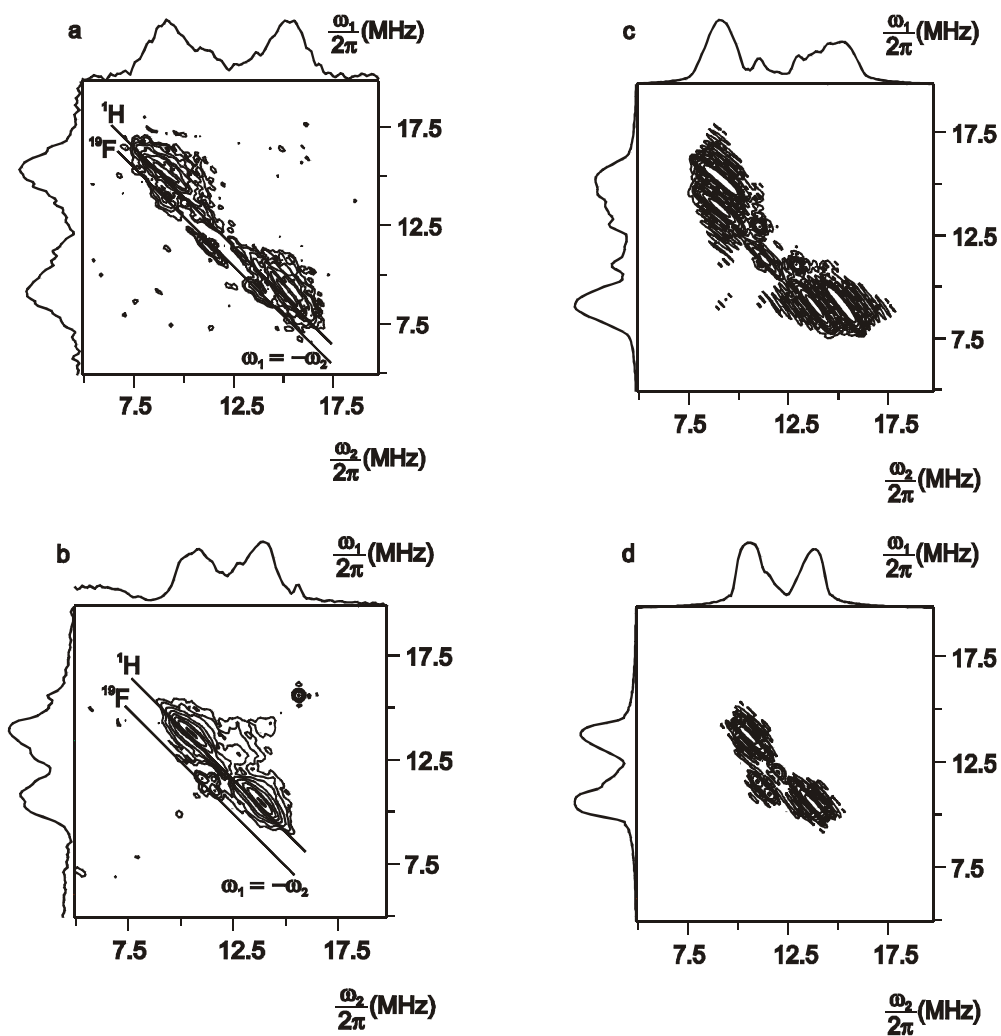


Figure S8. X- band HYSORE spectra of **S1** - $\text{Cu}(\text{OTf})_2/\text{tert}$ -butylbox (a – Experimental, c – Simulated) and **S3** - $\text{Cu}(\text{OTf})_2/\text{tert}$ -butylbox + Ethyl glyoxylate + 1,3 - Cyclohexadiene (b – Experimental, d – Simulated), measured at the g_{zz} Cu(II) EPR spectral position 281.5 mT at 4 K, with $\tau = 160$ ns

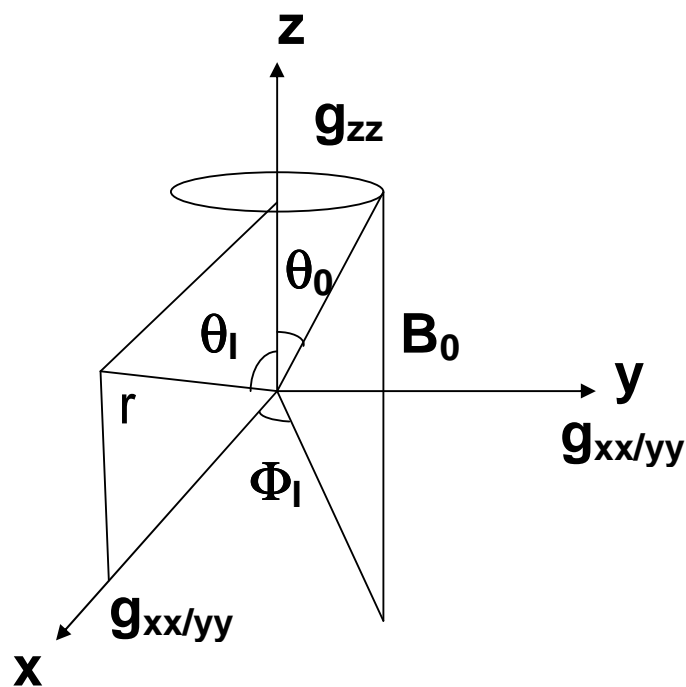


Figure S9. Vector diagram showing the relationship between the external field B_0 and the vector r joining the electron spin and the nucleus (^1H or ^{19}F) which lies in the xz plane. r is at an angle of θ_l to the z axis. The xyz coordinate frame corresponds to the g tensor frame. θ_0 is the angle between the external magnetic field B_0 and the g_{zz} axis. Φ_l is the azimuthal angle from z between the xz plane and the zB_0 plane.

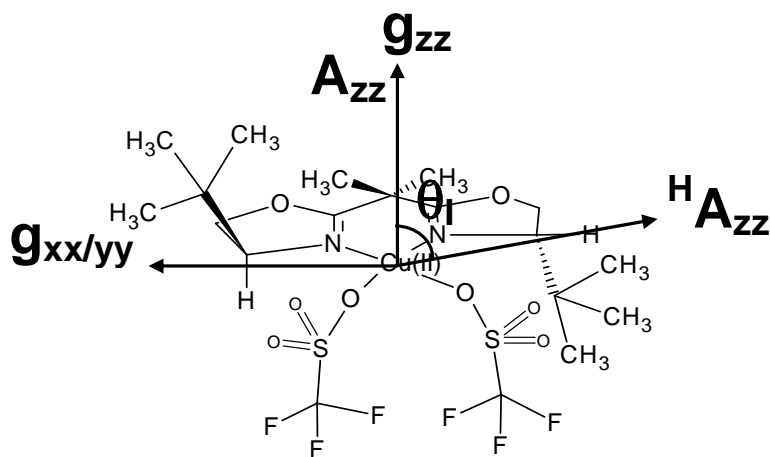


Figure S10. Schematic drawing of the $\text{Cu}(\text{OTf})_2/\text{tert}$ -butylbox complex (**S1**) together with the vector diagram showing the relationship between the \mathbf{g} tensor frame and the z axis of the proton hf tensor. The z axis of the proton hyperfine tensor is shown to be perpendicular to the \mathbf{g}_{zz} axis. The $\mathbf{g}_{xx/yy}$ and \mathbf{g}_{zz} axes of the Cu(II) \mathbf{g} tensor frame are respectively parallel and perpendicular to the complex plane containing Cu(II) ion, the two equatorially coordinated imine nitrogen atoms from the oxazoline rings of the *tert*-butylbox ligand, and the two equatorially coordinated oxygen atoms from the triflate ($-\text{O}-\text{SO}_2-\text{CF}_3$) (which are slightly tilted about 26° from the Cu(II) plane).

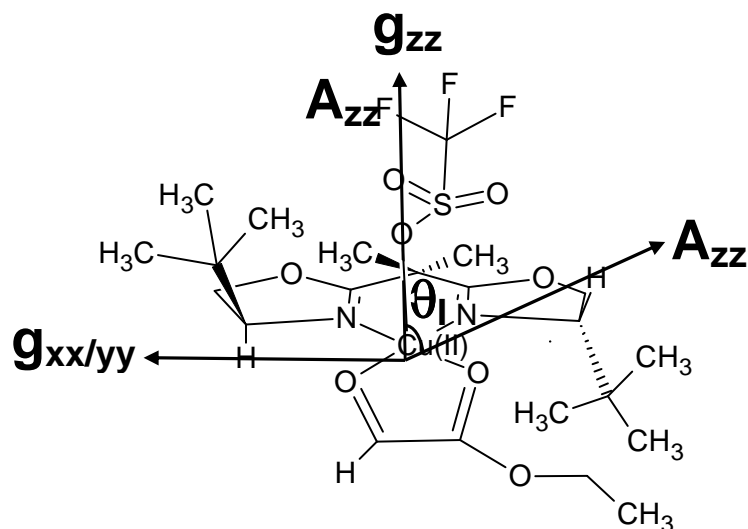


Figure S11. Schematic drawing of the $\text{Cu}(\text{OTf})_2/\text{tert}$ -butylbox + ethyl glyoxylate complex (**S2**) together with a vector diagram showing the relationship between the g tensor frame and the z axis of the proton hf tensor. The z axis of the proton hyperfine tensor is shown to be at an angle of 51° from the g_{zz} axis. The $g_{xx/yy}$ and g_{zz} axis of the Cu(II) g tensor frame are respectively parallel and perpendicular to the complex plane containing Cu(II) ion, two equatorially coordinated imine nitrogen atoms from the oxazoline rings of the *tert*-butylbox ligand and the two equatorially coordinated oxygen atoms from the dienophile (which are slightly tilted about 26° from the Cu(II) plane). Here the $-\text{OTf}$ ligands are axially coordinated to the Cu(II), through the sulphonic oxygen atom and is perpendicular to the complex plane containing Cu(II), and parallel to g_{zz} axis.

	g_{\perp}		g_{\parallel}	
	Exp	Calc	Exp	Calc
S1	2.077	2.067	2.303	2.208
S2	2.068	2.063	2.304	2.195
S3	2.080	2.072	2.323	2.198

Table S12. Comparison of calculated and experimental g-factors for **S1**, **S2** and **S3** structures.

	A_{\perp}				A_{\parallel}				A_{iso}			
	LP1	LP2	LP3/S2	sim	LP1	LP2	LP3/S2	sim	LP1	LP2	LP3/S2	sim
Cu	91.4	20.0	52.8	38.0	-411.2	-498.5	-536.6	424.0	-	-	-	-
N	25.6	33.0	35.7	35.0	35.1	44.7	48.6	35.0	28.6	37.1	40.3	35.0
H	-1.10	-0.48	-1.42	-1.46	-1.30	0.83	4.66	6.82	0.06	-0.04	0.50	1.3
F	1.58	0.07	-0.59	-0.73	-5.08	3.81	1.19	1.46	-2.61	1.11	0.00	0.00

Table S13. Comparison of calculated and experimental/simulated HFC couplings of Cu, N, relevant F and H nuclei for **LP1**, **LP2** and **LP3** structures.